JOURNAL OF MATERIALS SCIENCE 16 (1981) 2867–2876

The identification of faulted prismatic dislocation loops in single crystals of undoped InP

G. T. BROWN, B. COCKAYNE, W. R. MacEWAN
Royal Signals and Radar Establishment, St. Andrews Road, Malvern, Worcs, UK

High-voltage transmission electron microscopy has shown that undoped single crystals of indium phosphide, grown by the liquid-encapsulated Czochralski technique, can contain linear arrays of faulted dislocation loops. The plane of the loops is (1 1 0), the fault vector is $\frac{1}{n}$ [1 1 0] and the Burgers vector of the dislocation loop is $\frac{1}{n}$ [1 1 0]. A direct correlation has been obtained between these loops and arrays of both ridge and prism features revealed by chemical etching. Sequential use of two etchants has also established a direct link between the faulted dislocation loops and the slip dislocations induced by thermal stresses during crystal growth. A study of a number of crystals grown from differently prepared starting materials suggests that the formation of the loops is associated with departures from stoichiometry and inhibited by the presence of dopant impurities.

1. Introduction

Crystalline defects such as dislocations, when present in semiconducting single-crystal substrates, can limit the performance of devices made in epitaxial layers grown onto such substrates. Hence, the characterization and control of such defects can play an important part in improving the usefulness of the semiconductor. In earlier work, the present authors have shown that the dislocations present in single crystals of indium phosphide grown by the liquid-encapsulated Czochralski (LEC) technique, and used extensively as substrate material, arise from two main sources [1, 2]. These are dislocations induced by slip as a result of thermal stresses experienced during growth [1] and dislocations associated with inclusions or precipitates [2]. Minor sources of dislocations are the seed–crystal junction and growth striations [3]. Techniques for controlling the formation of most of these dislocations have also been established [2, 4]. Thus far, these defects have been studied mainly by revealing the dislocations as pits or ridges with chemical etchants and using X-ray transmission topography to correlate the etched structures with dislocations [2]. The present paper reports additional work in which some of the etched features are correlated with detailed dislocation structures observed by high-voltage transmission electron microscopy (HVEM). The results permit further comment to be made about the manner in which dislocations behave in indium phosphide single crystals.

2. Experimental procedure

The single crystals of InP studied herein were all grown by the liquid-encapsulated Czochralski (LEC) technique [5] incorporating automatic diameter control based on the crucible weighing method [6] and using starting materials and experimental procedures described fully in an earlier paper [7]. Both ⟨1 0 0⟩ and ⟨1 1 1⟩ axis undoped crystals were grown and typical figures for room-temperature carrier concentration and mobility were 3×10^{15} cm^{-3} and 4500 cm^2 V^{-1} sec^{-1}, respectively. {1 0 0} and {1 1 1} slices cut from these crystals were chemically polished on Pellon pads in a solution of 1 vol% bromine in methanol; up to 250 μm of material was removed to avoid effects due to residual work damage. It should be noted that for the {1 1 1} slices, only the

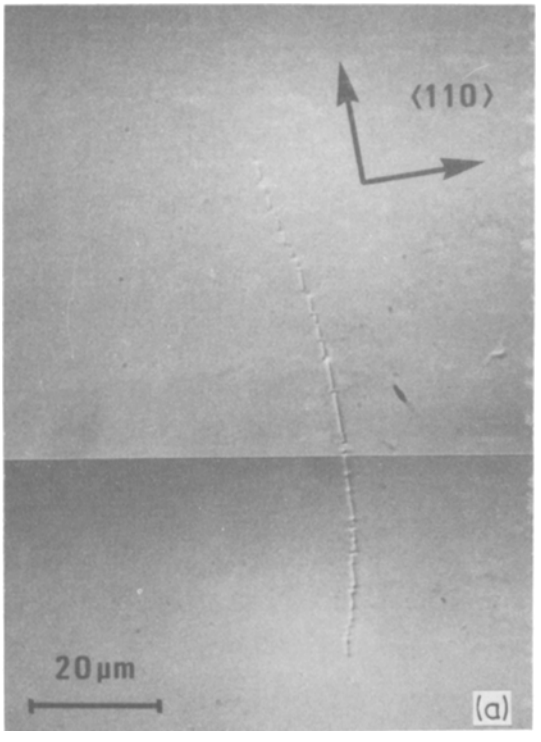

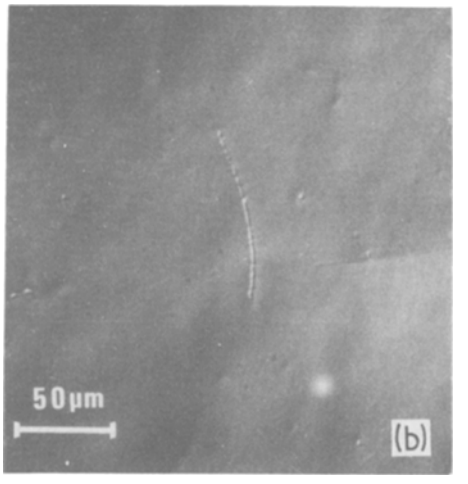

Figure 1 (a) An array of short straight ridge features produced on a {1 0 0} slice of an undoped crystal after etching for 10 min in Solution AB. (b) The same feature as shown in (a) at low magnification.

{1 1 1}P face can be examined as no chemical polish is known for the {1 1 1}In face. The {1 0 0} and {1 1 1}P faces were then etched in either Solution H [8] (electronic-grade orthophosphoric acid and hydrobromic acid in the volume ratio 2:1) or Solution AB [9] (1 g chromium trioxide, 8 mg silver nitrate dissolved in 2 ml of de-ionised water and 1 ml of hydrofluoric acid) under conditions defined in detail elsewhere [1]. A post-etching treatment in 10 vol% hydrochloric acid in water was introduced to remove the residue left on the surface by Solution AB.

Transmission electron microscopy (TEM) samples were prepared by ultrasonically trepanning 3 mm diameter discs from chemically-polished {1 0 0} slices, etched on one side only for 15 min in Solution AB. These discs were fastened to a Teflon block and masked with lacquer to leave a window on the unetched face of the disc. The window region was thinned to the point of perforation in a solution of 1 vol% bromine in methanol, after which such samples were cleaned in acetone and 2-*n*-propanol. The thinned samples were examined in an AEI-EM7 high-voltage electron microscope. In cases where high accelerating voltages (> 400 kV)

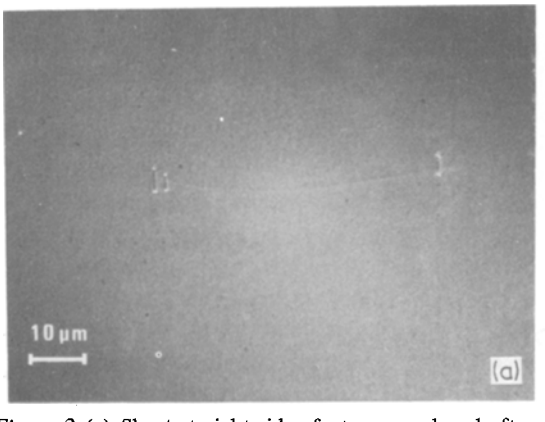

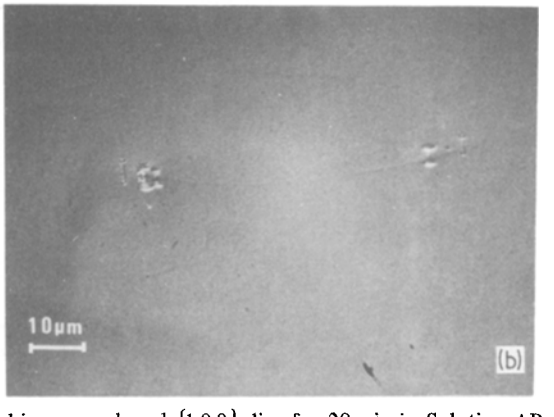

Figure 2 (a) Short straight ridge features produced after etching an undoped {1 0 0} slice for 20 min in Solution AB. (b) The same area shown in (a) after etching for a further 10 min in Solution AB, showing the production of more ridged features.

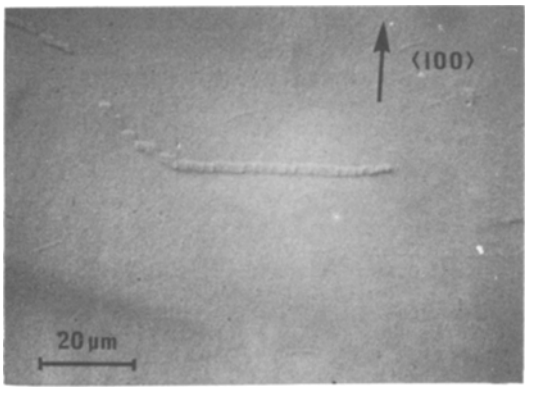

Figure 3 A vertical ⟨1 1 0⟩ section of an undoped ⟨1 0 0⟩ axis crystal which has been etched for 30 min in Solution AB, showing an array of ridged features.

were needed to penetrate large areas, the specimens were cooled to 150 K to minimize radiation damage.

3. Results

3.1. Chemical etching and optical microscopy

Our previous study [1] showed that etching {1 0 0} slices of InP, cut from undoped ⟨1 0 0⟩ axis crystals, in Solution AB produced a series of ridges which contained discontinuities and gave the ridges the appearance of being decorated. The present more detailed study shows clearly (Fig. 1) that the ridge features are composed of a set of discrete straight ridges with small etch pits at the end of each ridge which cause the apparent decoration effect. The short ridges are aligned along the ⟨1 1 0⟩ directions and are frequently arranged in linear arrays. Short straight ridges in isolation from other features are also observed. Further etching in Solution AB simply extends the arrays by the appearance of more discrete ridges, as shown in Fig. 2. This implies that the defects responsible for the ridges are also discrete. The presence of dislocation loops or precipitates would be consistent with these observations.

Examination of {1 1 0} vertical sections from undoped ⟨1 0 0⟩ axis crystals, after etching in Solution AB, also reveals the presence of ridged features in arrays, with edges parallel to the ⟨1 0 0⟩ growth axis and the ⟨1 1 0⟩ direction (Fig. 3). It seems likely, therefore, that the defect responsible for these features is similar or identical to the one which creates the short ridges in Fig. 1. A slight change in morphology is apparent be-

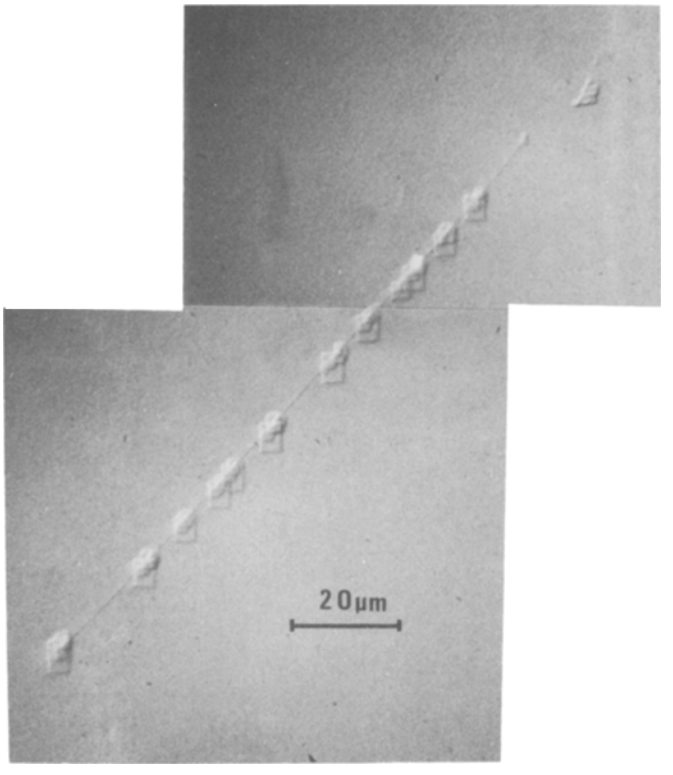

Figure 4 An array of rectangular prism features produced on a {1 0 0} slice taken from an undoped ⟨1 0 0⟩ crystal after etching for 30 min in Solution AB.

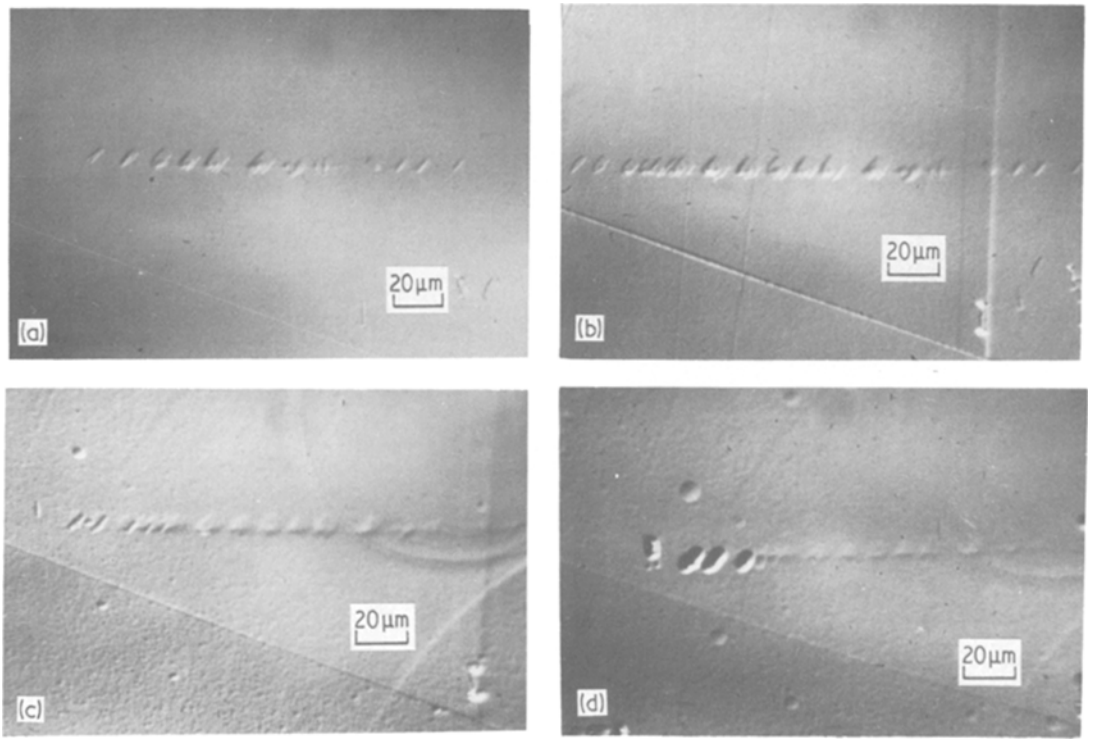

Figure 5 An array of rectangular prism features produced on a {1 0 0} slice of an undoped ⟨1 0 0⟩ axis crystal after etching in: (a) Solution AB for 10 min; (b) Solution AB for 20 min; (c) Solution AB for 20 min followed by Solution H for 30 sec; (d) Solution AB for 20 min followed by Solution H for 40 sec.

tween the two cases and the etch pits at the end of the short ridges on the {1 0 0} surfaces are replaced by additional ridges on the {1 1 0} surfaces.

A second type of etch feature was observed on {1 0 0} slices of undoped material etched in Solution AB. This is a rectangular-prism type of feature which is attached to neighbouring prisms by a parent ridge to form the linear arrays seen in Fig. 4; the prism edges are parallel to the ⟨1 0 0⟩ directions. On further etching in Solution AB, the arrays extend by the revelation of new prisms at one end whilst the prisms at the end of the array that intersects the surface grow larger (see Fig. 5a and b). These effects establish that the defects responsible for the prism features are inclined to the surface.

The behaviour of the {1 1 1}P compared to the {1 0 0} surfaces, when etched in Solution AB, has

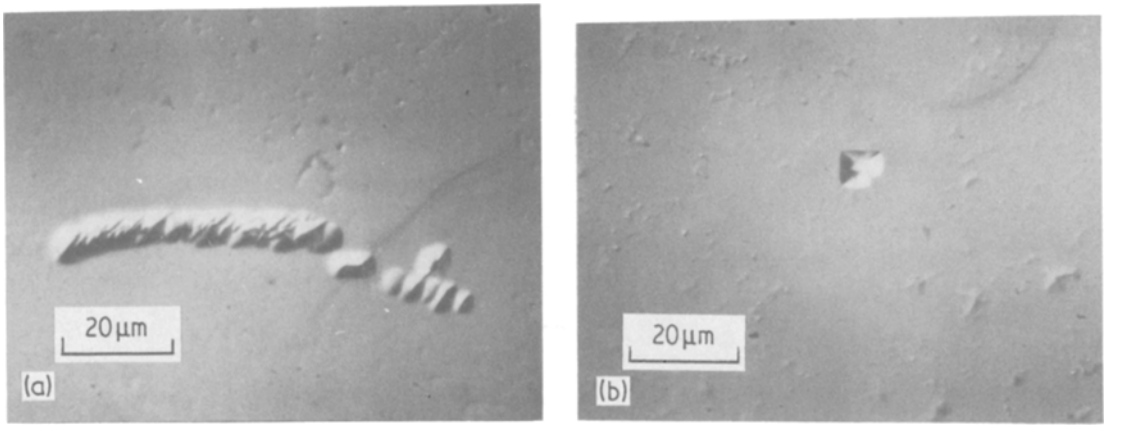

Figure 6 A {1 0 0} surface taken from an undoped ⟨1 0 0⟩ axis crystal after etching for 10 sec in Solution H, showing: (a) a line of closely associated pits; (b) isolated rectangular pits.

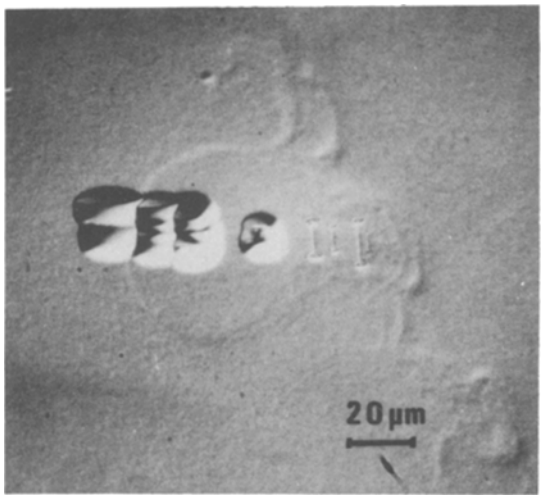

Figure 7 Correlation between the rectangular pits produced on a {1 0 0} slice of an undoped ⟨1 0 0⟩ axis crystal after etching for 40 sec in Solution H and short ridge features produced after etching for 20 min in Solution AB.

Figure 8 (a) An off-set linear array of short ridges on the etched side of a high-voltage electron microscope specimen. (b) The same area in the high-voltage electron microscope at 800 kV showing an off-set linear array of stacking faults.

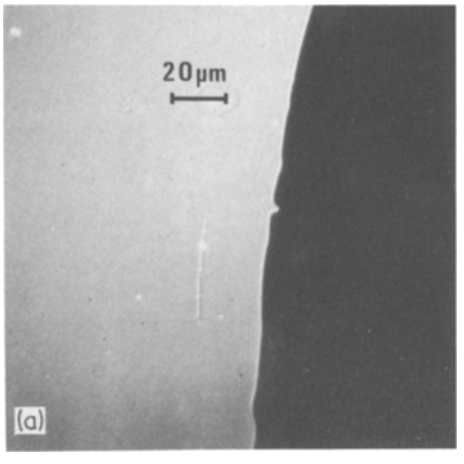

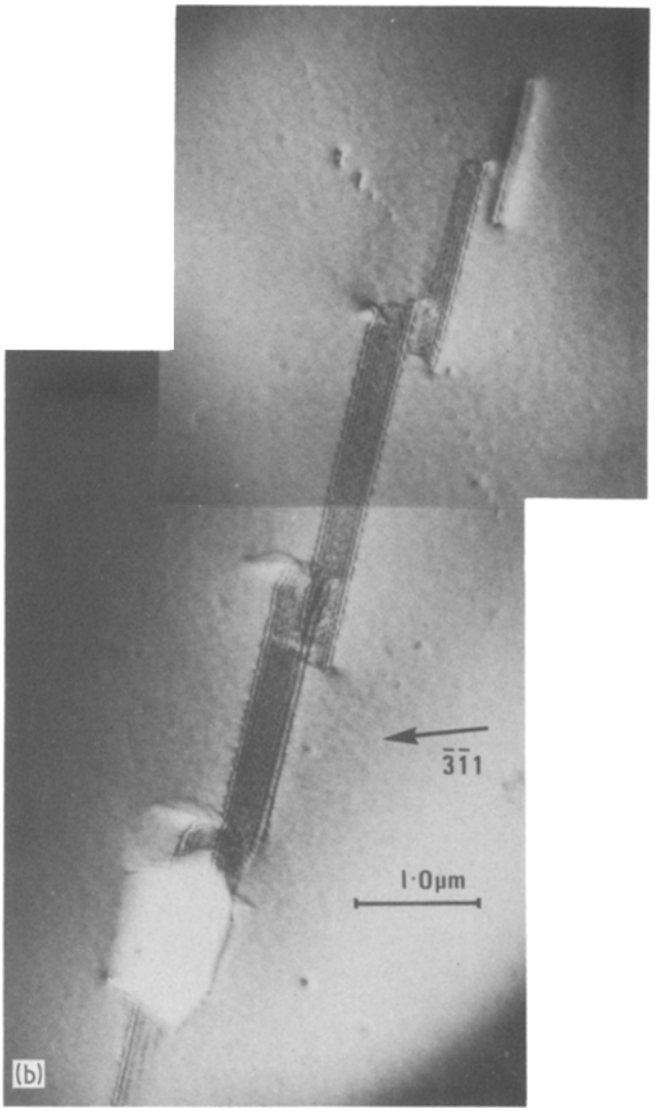

been described in a previous study [1]; the major difference seen between the two surfaces is that {1 1 1}P surfaces develop both etch pits and ridged arrays. This study has confirmed that {1 1 1}P surfaces cut from ⟨1 1 1⟩ axis undoped crystals contain these features but has further shown that the arrays consist of short straight ridges identical to those in Fig. 1 except that for {1 1 1}P surfaces the ridges are aligned along the ⟨1 1 2⟩ directions.

An alternative chemical etchant for InP, Solution H, behaves more conventionally than Solution AB, producing pits where defects emerge at the surface. The previous study [1] showed that two types of pits are revealed by this etchant on both {1 1 1}P and {1 0 0} surfaces, namely, conical pits and flat-bottomed pits. The present study of undoped material has shown that two further features can develop for both surfaces; these are isolated rectangular pits and lines of closely associated pits (Fig. 6). By etching with the Solutions

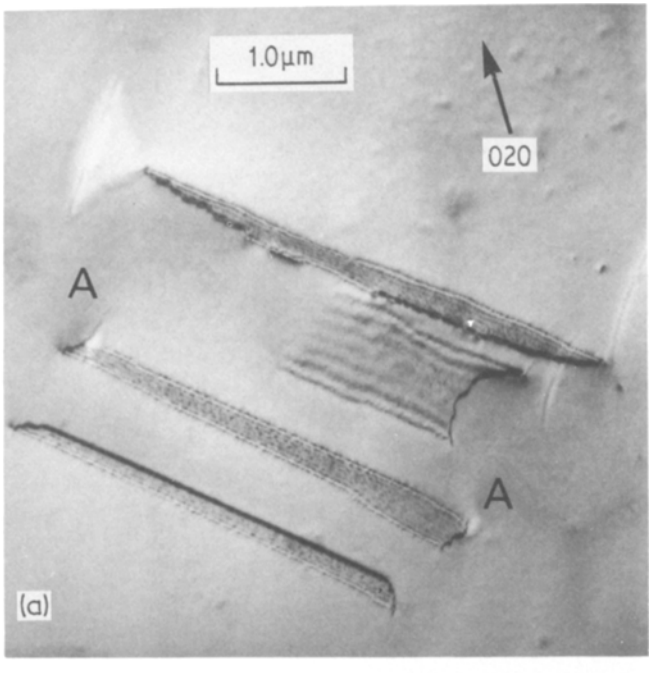

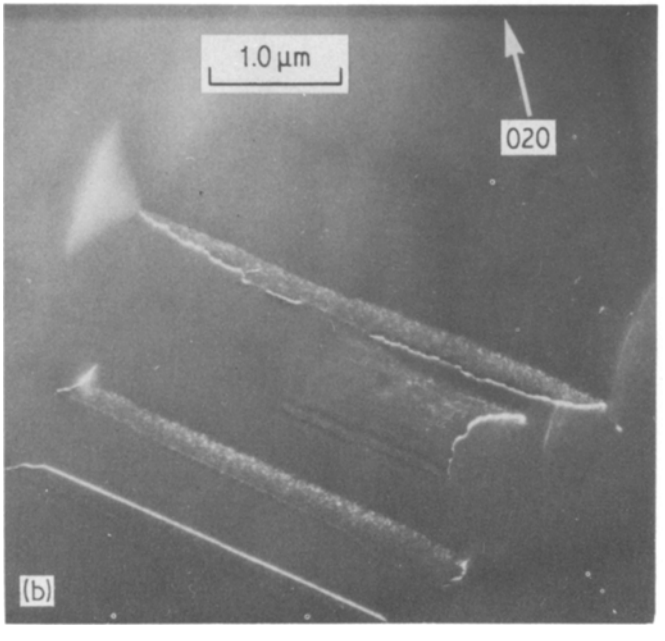

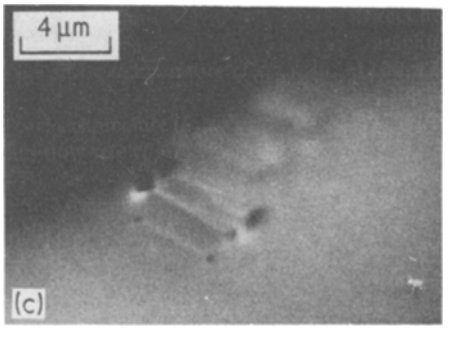

Figure 9 Micrographs of an array of stacking faults in a sample taken from an undoped crystal and imaged (a) in the high-voltage electron microscope at 400 kV using bright-field diffracting conditions; (b) as (a) but using $g3g$ weak-beam diffracting conditions and (c) in a scanning electron microscope at 20 kV with back-scattered electrons.

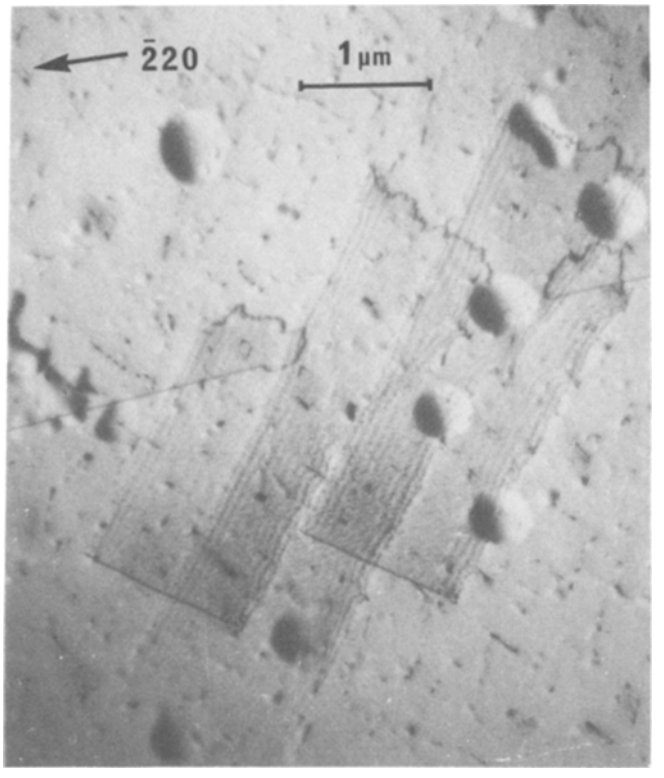

Figure 10 Micrograph of a group of stacking faults taken in the high-voltage electron microscope at 800 kV with a beam direction close to [0 0 1].

AB and H sequentially on a {1 0 0} surface (Fig. 5c and d) it can be seen that rectangular etch pits are produced by Solution H at the points where the raised rectangular prism features, produced by Solution AB, intersect the surface. Fig. 7 shows that an identical correlation can be achieved between arrays of rectangular pits produced by Solution H and the arrays of short straight ridges produced by Solution AB and shown in Fig. 1.

Hence, a direct correlation exists between the features revealed by Solutions AB and H; the lines of pits formed by Solution H correspond to the linear arrays of straight ridges or the raised rectangular prisms induced by Solution AB whilst the isolated rectangular pits formed by Solution H correspond to isolated ridges or prisms induced by Solution AB.

3.2. Correlation of etch features with TEM

High-voltage transmission electron microscopy has been used in conjunction with etching in Solution AB to identify the defect responsible for the new etch features outlined above. The optical micrograph of Fig. 8a shows an off-set linear array of straight ridge features, of the type reported in Fig. 1, close to the edge of a thinned foil. A high-voltage transmission electron micrograph of this area, shown in Fig. 8b, shows that this array is a string of stacking faults. Another example, this time with the stacking faults arranged side-by-side, is shown in Fig. 9a, but in this instance a high-magnification scanning electron microscope has been used to show the detailed surface features produced by etching in Solution AB (Fig. 9c). The pits which form at the end of each ridge, typified by AA, correlate directly with the dislocations present at the ends of each fault. Fig. 9a also shows that the top and bottom of both the lowest and uppermost faults are bounded by dislocation lines which are very nearly linear; this infers that the defects responsible for these etch features are faulted dislocation loops elongated in the ⟨1 1 0⟩ directions. This explains the etching behaviour because, when such defects are attacked by Solution AB, a ridge is formed at the top of the fault where the bounding dislocation is virtually parallel to the surface whilst a pit is formed at the edges of the faulted loop where the bounding dislocation is almost perpendicular to the surface.

A similar correlation exercise was carried out for the rectangular prism features and the electron micrograph in Fig. 10 shows a group of stacking faults which correspond to a feature equivalent to those shown in Fig. 4. The parent

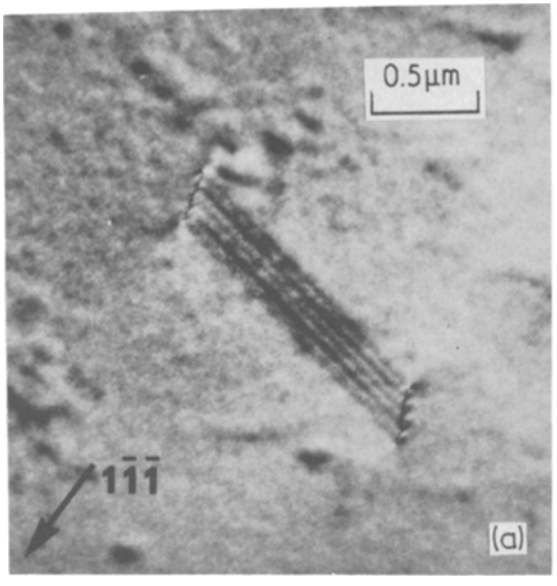

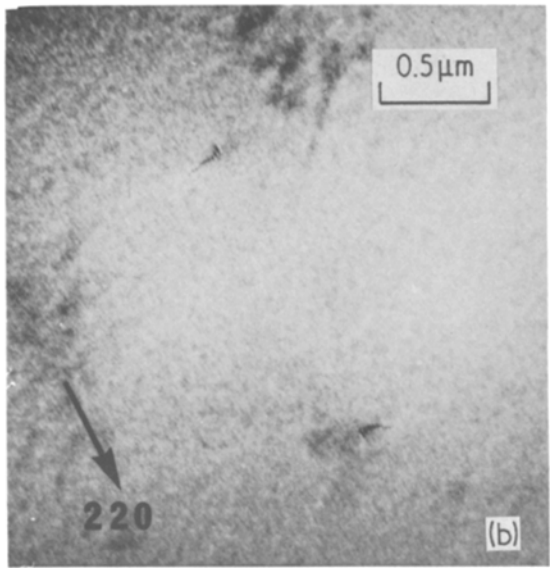

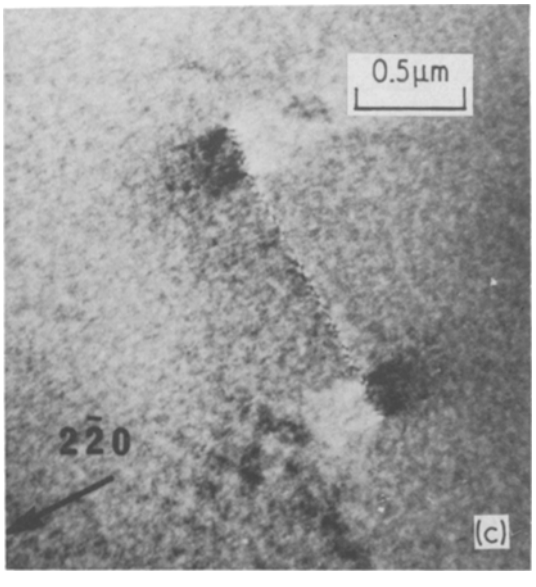

Figure 11 Micrographs of a stacking fault taken in the high-voltage electron microscope at 400 kV with: (a) beam direction close to [1 0 1]; (b) beam direction close to [$\bar{2}$ 2 5]; (c) beam direction close to [1 1 2].

ridge which connects the prisms in the array can be identified in the micrograph as a dislocation line connecting groups of faults, and the fine structure within each prism is clearly due to a group of stacking faults in close proximity.

3.3. Analysis of the faulted loops

The displacement vector for the fault shown in Fig. 11 was determined using the invisibility criterion; the fault was out of contrast for [$\bar{1}$ $\bar{1}$ 1] and [2 2 0] diffraction vectors (see Fig. 11b) which defined the fault vector as $\frac{1}{n}$ [$\bar{1}$ 1 0]. The fault was vertical in the foil (Fig. 11c) along the [$\bar{1}$ 1 0] zone (i.e., for [1 1 2] and [0 0 1] beam directions) which defines the fault plane as ($\bar{1}$ 1 0). The bounding dislocations follow the same contrast behaviour as the fault vector and hence the Burgers vector is $\frac{1}{n}$ [$\bar{1}$ 1 0]. However, as Fig. 11 shows, in some cases the dislocations are dissociated and the stacking fault adjoining the bounding partial dislocations remains in contrast.

The faults in Fig. 10 also lie on {1 1 0} planes with a ⟨1 1 0⟩ fault vector but in this case the {1 1 0} planes are those which are inclined to the {0 0 1} surface plane.

Figs 8 and 9 reveal one further point concerning the faulted loops in that the bright-field fringe contrast shows a certain spottiness. If this effect is examined using weak-beam diffraction conditions (Fig. 9b), it is clear that the faulted loops are decorated with either very small loops or precipitates (of size 10 to 20 nm); thus far, it has not proved possible to determine the precise nature of this decoration.

3.4. The source of the faulted loops

Our earlier study [1] showed that the pattern of etch pits produced by Solution H on {1 0 0} surfaces cut from ⟨1 0 0⟩ axis crystals and on {1 1 1}P surfaces cut from ⟨1 1 1⟩ axis crystals was consistent with the majority of dislocations originating from slip caused by thermal stresses generated as the grown crystal cooled. In this study, a {1 0 0}

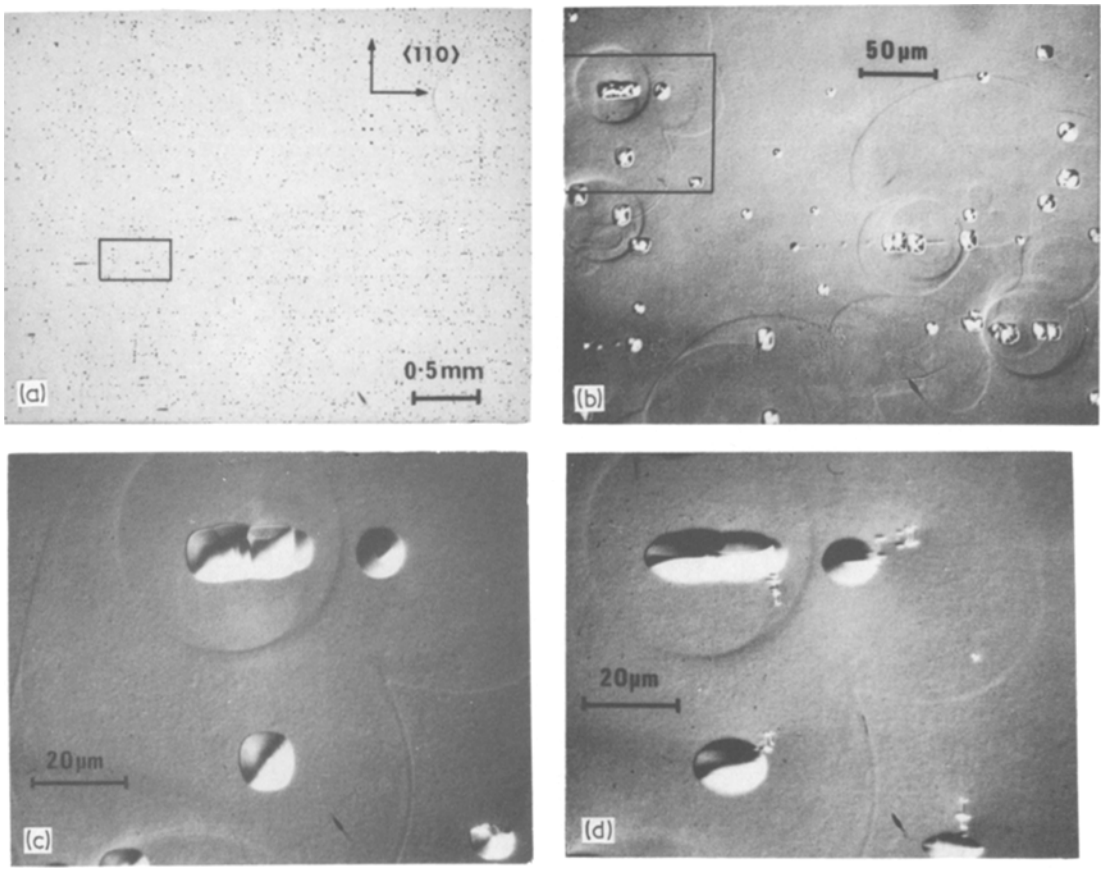

Figure 12 {1 0 0} surface of undoped ⟨1 0 0⟩ axis crystal: (a) etched in Solution H for 30 sec showing alignment of etch pits in ⟨1 1 0⟩ directions; (b) higher magnification of the area marked in (a); (c) higher magnification of the area marked in (b); (d) the same area as (c) but etched for a further 30 min in Solution AB showing the formation of ridge features at the original pits.

slice cut from a ⟨1 0 0⟩ axis undoped crystal showed an etch-pit pattern characteristic of slip dislocations when etched in Solution H (see Fig. 12a). Sequential etching of this slice in Solution AB established that the pits responsible for this slip pattern are associated with the arrays of short straight ridges, shown previously to be faulted loops (see Fig. 12b, c and d). It can be inferred, therefore, that the faulted loops originate on dislocations introduced by slip.

3.5. The size and distribution of the faulted loops

Examination of a number of loops using high-voltage electron microscopy established that the typical dimensions for the fault were within the range 2 to 6 μm. The density and distribution of the faulted loops is substantially similar to that of the original slip dislocations which is to be expected from the correlation established in the preceding section.

In this study, six undoped crystals have been examined in detail. Four of these were grown directly from polycrystalline starting material, which is normally very slightly rich in In, and all four of these crystals contained faulted loops. A fifth crystal was grown from polycrystalline material prepared under conditions which yielded no observable excess In, whilst the remaining crystal was prepared from stoichiometric single crystals; neither of these latter crystals contained faulted loops. Seven doped crystals have also been examined, doped variously with Ge (10^{16} to 10^{19} carriers cm^{-3}), Cr, Fe and Co (all up to approximately 5×10^{16} atoms cm^{-3}); no faulted loops were detected in any of these samples.

4. Discussion

The preceding observations clearly demonstrate that the defects responsible for the linear arrays of straight ridges and raised rectangular prisms, produced after etching single-crystal InP in

Solution AB, are faulted, prismatic dislocation loops. Both of these groups of features lie on the {1 1 0} planes and their difference in appearance on the {1 0 0} surfaces is consistent with the plane of the loop lying perpendicular to the {1 0 0} surface for the ridges but inclined at an angle to this surface for the prisms.

The faulted loops are arranged in arrays which follow closely the original course of dislocation lines. In fact, for the raised rectangular prism features, the original dislocation line can be seen between the loops (see Figs 4 and 10). The correlation established between the features and the etch-pit pattern produced by Solution H, which is characteristic of dislocations generated by thermal stresses inherent in Czochralski crystal growth, indicates a direct link between the original slip dislocations and the faulted loops. The precise mechanism of this change is not yet established but it is obviously derived from the thermal annealing which occurs as the crystal both grows and cools and must involve diffusion processes.

The wide-spread occurrence of faulting in nominally undoped single crystals, grown from starting material which is slightly indium rich, and an apparent absence of faulting in a limited examination of undoped crystals prepared from stoichiometric starting material and doped crystals suggests that the formation of the faulted loops is associated with departures from stoichiometry but is inhibited by the presence of impurities. In InP, departures from stoichiometry invariably occur by loss of phosphorus during preparation, leading to the formation of either phosphorus vacancies or indium interstitials. The precipitation of either of these defects at dislocation sites could promote the formation of faulted loops.

Finally, it should be noted that no evidence has been obtained during this work to suggest any common cause between the faulted prismatic loops observed here and the prismatic loops described in an earlier study [2] which are derived from the incorporation of an inclusion or a precipitate.

Acknowledgements

The authors would like to thank Miss S. Ruddock and Mr E. Bullen for their help with specimen preparation, Mr D. G. Coates for the SEM work and Birmingham University for the provision of the high-voltage electron microscope facility. This paper is published by permission of the Copyright © Controller, HMSO, London, 1981.

References

1. G. T. BROWN, B. COCKAYNE and W. R. MacEWAN, *J. Mater. Sci.* **15** (1980) 2539.
2. B. COCKAYNE, G. T. BROWN and W. R. MacEWAN, *J. Crystal. Growth* **51** (1981) 461.
3. G. T. BROWN, B. COCKAYNE and W. R. MacEWAN, Proceedings of the 2nd Oxford Conference on Microscopy of Semiconductors, Oxford, Institute of Physics Conference Series (Institute of Physics, London), to be published.
4. *Idem, J. Crystal Crowth* **51** (1981) 369.
5. J. B. MULLIN, A. ROYLE, B. W. STRAUGHAN, Proceedings of the International Symposium on GaAs and Related Compounds, Aachen, 1970 (Institute of Physics, London) p. 71.
6. W. BARDSLEY, B. COCKAYNE, G. W. GREEN, D. T. J. HURLE, G. C. JOYCE, J. M. ROSLINGTON, P. J. TUFTON and H. C. WEBBER, *J. Crystal Growth* **24/25** (1974) 39.
7. B. COCKAYNE, W. R. MacEWAN and G. T. BROWN, *J. Mater. Sci.* **15** (1980) 2785.
8. A. HUBER and N. T. LINH, *J. Crystal Growth* **29** (1975) 80.
9. M. ABRAHAMS and C. J. BUIOCCHI, *J. Appl. Phys.* **36** (1965) 2855.

Received 27 February and accepted 26 March 1981.